Electronic Supplementary Information (ESI) for 'Quantifying DNA-Mediated Liposome Fusion Kinetics with a Fluidic Trap'

Rodolphe Marie,* Martin K. Rasmussen, and Jonas N. Pedersen

Department of Health Technology

Technical University of Denmark

2800 Kongens Lyngby, Denmark

E-mail: R.M:rcwm@dtu.dk

Diffusiophoretic trapping mechanism

The theory behind diffusiophoretic trapping in a nanofluidic chip is described in detail elsewhere,[1,2] but it is here outlined for completeness.

Diffusioosmosis and diffusiophoresis

In a salt gradient, the diffusiophoretic particle velocity is[3]

$$v_{\mathrm{ph}}(x) = \Gamma_{\mathrm{ph}}(\zeta, d)\frac{\nabla C(x)}{C(x)}, \tag{ESI-1}$$

where $C(x)$ is the salt concentration at position x, and Γ_{ph} is the diffusiophoretic mobility which depends on the particle diameter d and zeta potential ζ. Expanding Γ_{ph} to first order

in $\lambda = \lambda_{\mathrm{DB}}/(d/2)$ gives [3]

$$\Gamma_{\mathrm{ph}} = \frac{\epsilon}{2\eta}\left(\frac{k_{\mathrm{B}}T}{Ze}\right)^2 \left[u_0 + \lambda u_1\right], \tag{ESI-2}$$

where $\lambda_{\mathrm{DB}} = \sqrt{\epsilon k_{\mathrm{B}}T/(2e^2 N_A I)}$ is the Debye length, ϵ is the permittivity of the medium, η is the dynamic viscosity, Z is the valence of the solute, I is the ionic strength, e is the elementary charge, $u_0 = 2\beta\frac{Ze\zeta}{k_{\mathrm{B}}T} - 4\ln\left(1-\gamma^2(\bar{\zeta})\right)$, and $u_1 = F_0 + \beta F_1 + \mathrm{Pe}\left[F_2 + \beta\left(F_3 + F_5\right) + \beta^2 F_4\right]$. Furthermore, $\mathrm{Pe} = \frac{\epsilon}{2\eta D}\left(\frac{k_{\mathrm{B}}T}{Ze}\right)^2$, $\gamma(\bar{\zeta}) = \tanh(\bar{\zeta}/4)$, $\bar{\zeta} = Ze\zeta/(k_{\mathrm{B}}T)$, $\beta = \left(D_+ - D_-\right)/\left(D_+ + D_-\right)$, and $D = 2D_+D_-/(D_+ + D_-)$, where D_+ and D_- are the diffusion coefficient of the cations and anions of a monovalent salt, respectively. The dominant ions in PBS are sodium ions Na^+ with $D_{\mathrm{Na}^+} = 1330\,(\mu\mathrm{m})^2\,\mathrm{s}^{-1}$ and chloride ions Cl^- with $D_{\mathrm{Cl}^-} = 2030\,(\mu\mathrm{m})^2\,\mathrm{s}^{-1}$, hence $\beta \simeq -0.20$ for NaCl.[3] The F-functions depend on $\bar{\zeta}$ and are tabulated in Table 2 in Reference [3]. Notice that the Debye length changes across the channel as it depends on the ionic strength I, and hence the concentration of the solute.

The diffusioosmotic slip velocity due to a salt gradient in bulk near a charged wall is [3]

$$v_{\mathrm{slip}}(x) = -\Gamma_{\mathrm{os}}(\zeta_{\mathrm{ch}})\frac{\nabla C(x)}{C(x)}. \tag{ESI-3}$$

Here $\Gamma_{\mathrm{os}}(\zeta_{\mathrm{ch}}) = \frac{\epsilon}{\eta}\frac{k_{\mathrm{B}}T}{Ze}\left[\beta\zeta_{\mathrm{ch}} - 2\frac{k_{\mathrm{B}}T}{Ze}\ln\left(1-\gamma^2(\bar{\zeta}_{\mathrm{ch}})\right)\right]$ is the diffusioosmotic mobility with ζ_{ch} the zeta potential of the channel wall. In a nanochannel, the diffusioosmotic slip velocity causes a constant fluid flow rate Q due to conservation of mass,[4] and if the nanochannel width varies slightly compared to the length ($\Delta w/L \ll 1, \Delta w = w_W - w_N$), the flow rate is assumed to be [1,4]

$$Q = w(x)h v_{\mathrm{slip}}(x) - \frac{w(x)h^3\partial_x P(x)}{12\eta}. \tag{ESI-4}$$

Here $w(x) = w_N + (w_W - w_N)x/L$ is the width of the nanochannel at position x, where x is measured along the nanochannel starting at the narrow end, and $\partial_x P(x)$ is the internal pressure gradient along the nanochannel. Assuming that the pressures are identical on both sides of the nanochannel, we set $P(0) = P(L)$, divide both sides of eqn (ESI-4) by $w(x)$, and

integrate from 0 to L. So the diffusioosmotic flow rate in the nanochannel is[1]

$$Q = \frac{\Gamma_{\rm os}(\zeta_{\rm ch}) \ln\left(C_N/C_W\right) h\Delta w}{L \ln\left(1+\Delta w/w_N\right)}, \tag{ESI-5}$$

and the diffusioosmotic fluid velocity is

$$v_{\rm os}(x) = \frac{Q}{hw(x)}. \tag{ESI-6}$$

As in References[1,2], we determine the flow rate Q from a calibration of the device. By recording a steady state concentration of a dye in the nanochannel when it is introduced in one of the microchannels, it is found that $Q = 450\,\mathrm{fL\,min^{-1}}$ at the present experimental conditions.[1,4]

Hydrodynamic radius of a sphere between infinite walls

The diffusion coefficient of a sphere with diameter d is in bulk $D_0 = k_B T/(3\pi\eta d)$, where η is the viscosity of the medium. In eqn (3) in the main text, D_p is the diffusion coefficient of a particle confined in a nanochanel. We approximate this diffusion coefficient with the one for a particle moving midway between infinite walls separated by a distance h.

In the Faxén approximation that is [see Reference[5], eqn (7-4.27)]

$$D_p^{\rm Faxén}(d/h) = D_0\left[1 - 1.004\left(\frac{d}{h}\right) + 0.418\left(\frac{d}{h}\right)^3 + 0.21\left(\frac{d}{h}\right)^4 - 0.169\left(\frac{d}{h}\right)^5\right], \tag{ESI-7}$$

which shows good agreement with experimental data for $d/h \lesssim 0.6$.[6] The so-called Oseen superposition is a better approximation for larger values of d/h,[7]

$$\frac{D_0}{D_p^{\rm Oseen}(d/h)} = \frac{2}{1 - \frac{9}{16}\frac{d}{h} + \frac{1}{8}\left(\frac{d}{h}\right)^3 - \frac{45}{256}\left(\frac{d}{h}\right)^4 - \frac{1}{16}\left(\frac{d}{h}\right)^5} - 1, \tag{ESI-8}$$

but the two approximations agree for $d/h \lesssim 0.6$, i.e., the limit of interest for the present

liposome data. When fitting the intensity profile for the fusion products, we only use the Oseen approximation.

Nanofluidic trapping theory

If the concentration of buffers are C_N and C_W at the narrow and wide end of the nanochannel, respectively, the concentration inside the nanochannel is[1]

$$C(x) = C_N + (C_W - C_N)\ln[w(x)/w_N]/\ln[w_W/w_N]. \tag{ESI-9}$$

The size and zeta potential of the trapped particles can be determined from their distribution along the nanochannel, see eqn (3) in the main text. This was previously demonstrated for vesicle diameters up to $\sim 63\%$ of the channel height when benchmarked against DLS measurements for the size and laser Doppler electrophoresis (LDE) for the zeta potential (Fig. 3d in Reference[1]). In the present experiment, the size of the fusion product is expected to be approximately $\bar{d}_{\text{before}}\sqrt{2}$, i.e., 60% of the channel height.

The effective length of the trap is estimated from the distribution of trapped liposomes before fusion using the definition

$$L_{\text{trap}} = \int_{-\infty}^{\infty} dx \left\{ [w(x)/w(x_0)] \exp\left[\int_{x_0}^{x} dx' \, [v_{\text{os}}(x') + v_{\text{ph}}(x')]/D_p \right] \right\} \tag{ESI-10}$$

with $\bar{d}_{\text{before}}$ and $\bar{\zeta}_{\text{before}}$ as the diameter and zeta potential.[1] This gives $L_{\text{trap}} = 8.7\,\mu$m, i.e., approximately the full width at half maximum of the distribution in the upper panel in Fig. 4(b) in the main text. The different number of DNA molecules per liposome influence the trapping profile due to the different zeta potentials, but the difference in trapping volume is insignificant.

Fusion rates in bulk

The fusion rate $r^M_{\text{fusion}} = 1.7\,(\mu\text{M})^{-1}\,\text{s}^{-1}$ for 100 DNA probes per liposome stated in the main text is here compared to literature values for fusion experiments in bulk that detect lipid mixing.

In bulk, the kinetic equation for the second-order irreversible reaction, $A + D \underset{r^M_{\text{fusion}}}{\longrightarrow} AD$ is

$$\frac{dc_{AD}(t)}{dt} = r^M_{\text{fusion}} c_A(t) c_D(t) = r^M_{\text{fusion}} \left[c^0_A - c_{AD}(t)\right] \left[c^0_D - c_{AD}(t)\right], \tag{ESI-11}$$

where c_A, c_D, and c_{AD} denote molar concentrations, and $c^0_A = c_A(0)$ and $c^0_D = c_D(0)$.

For $c^0_A \neq c^0_D$ and the initial condition $C_{AD}(0) = 0$, the solution is

$$c_{AD}(t) = c^0_A + \frac{c^0_D - c^0_A}{1 - \frac{c^0_D}{c^0_A} \exp\left[(c^0_D - c^0_A) r^M_{\text{fusion}} t\right]}. \tag{ESI-12}$$

Note that $c_{AD}(t) \to c^\infty_{AD} = \min(c^0_A, c^0_D)$ for $t \to \infty$. That is, the fusion process stops when the limiting vesicle type has been used.

The half-maximum is reached when $c_{AD}(t) = c^\infty_{AD}/2$, which gives that

$$t_{1/2} = \frac{\ln\left[\frac{c^0_A(2c^0_D - c^\infty_{AD})}{c^0_D(2c^0_A - c^\infty_{AD})}\right]}{(c^0_D - c^0_A)\, r^M_{\text{fusion}}}. \tag{ESI-13}$$

In Reference[8] they used a lipid mixing assay with 100 nm-diameter DOPE/DOPC/CH vesicles with the same composition and double-anchored DNA probes (ds-1/4 and ds-2/3) as in the present study. Both kind of vesicles had $n = 100$ DNA probes, but one kind contained both FRET donors and acceptors. Fusion caused an increase in donor emission due to a decrease in FRET efficiency. The initial concentrations of labelled and unlabelled vesicles were 0.6 nM and 2.4 nM, respectively. If the experimental measurements in bulk were consistent with the second-order kinetics described by eqn (ESI-12) and the fusion rate was $k_M = 170\,\text{M}^{-1}\,\text{s}^{-1}$ with $n = 100$, so $r^M_{\text{fusion}} = k_M n^2 = 1.7\,(\mu\text{M})^{-1}\,\text{s}^{-1}$, then we predict a

half-time equal to $t_{1/2} = 183\,\mathrm{s} \sim 3\,\mathrm{min}$.

The black curve in Fig. 1A in Reference[8] shows the change in donor intensity for total lipid mixing, $I_D(\%) = 100 \times (I_t - I_0)/(I_{\mathrm{total}} - I_0)$. Here I_0 is the donor intensity at $t = 0$ before lipid mixing, and I_{total} the donor intensity after disruption of the vesicles. Donor intensities were measured with a spectrofluorometer.

The data for $I_D(\%)$ cannot be fitted with the second-order kinetics described by eqn (ESI-12), and $I_D(\%)$ does not saturate within the measurement time but reaches $> 90\%$ after 30 min. The 50 %-value is reached after $\sim 2.5\,\mathrm{min}$. The inner leaflet and content mixing shown in Fig. 1B and 2A (black curves) in Reference[8] happen on a similar time scale, but the maximum values reach only $\sim 50\%$ and $\sim 17\%$ of the maximum value within the measurement time of 30 and 60 minutes, respectively.

In conclusion, our estimate for the half-time ($\sim 3\,\mathrm{min}$) based on the fusion rate in the trap is in reasonable agreement with the half-times measured in bulk ($\sim 2.5\,\mathrm{min}$). Similar time scales were also observed by others in experiments in bulk with a comparable number of DNA strands per vesicle ($n = 50$) and total vesicle concentration (2.8 nM) (Fig. 5B and 6B in Reference[9]).

Shape of fusion products

Here we discuss the shape of various fusion products and their hydrodynamic radii in bulk. It is assumed that liposome fusion only involves two vesicles. For details, see also the main text.

Figure ESI-2 shows the original liposome with a diameter $\bar{d}_{\mathrm{before}} = 124\,\mathrm{nm}$ and three different fusion products. They are placed in a channel with height $h = 295\,\mathrm{nm}$ and drawn to scale. The surface area of the initial, spherical liposome is A_{before} and the volume is V_{before}. All fusion products have a surface area of $2A_{\mathrm{before}}$.

The spherical fusion product is not volume-conserving but has a volume $2\sqrt{2}V_{\mathrm{before}}$. The

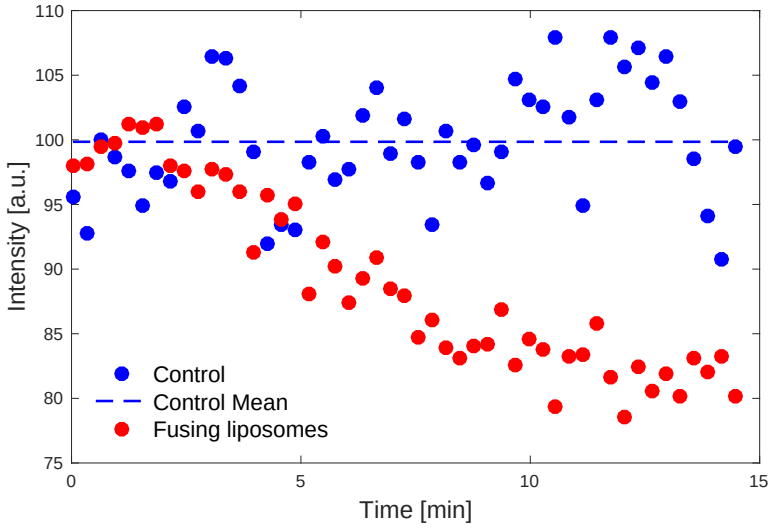

Figure ESI-1: Fluorescence intensity of liposomes with 50 DNA probes where 50% are hybridized with an Atto-590 labeled target (blue, 'Control'). The fluorescence intensity from the Atto-590 labels is constant (dashed blue line, 'Mean'). Fluorescence intensity of the same liposomes after exposure to liposomes with complementary DNA probes, resulting in a decreasing Atto-590 signal that reaches a plateau after $\sim$ 10 minutes (red, 'Fusing liposomes').

shape of the fusion product with conserved volume (surface area $2A_{\text{before}}$ and volume $2V_{\text{before}}$) is calculated using the spontaneous curvature model for zero spontaneous curvature (red).[10] For diffusion in bulk, approximate analytical methods exist for calculating the hydrodynamic radius of particles with arbitrary shapes,[11] but here we approximate the shape of the volume-conserving fusion product with a prolate ellipsoid with the same surface area and volume (purple figure). The length of the semimajor and semiminor axes are $b = 0.404\,\bar{d}_{\text{before}}$ and $a = bp$ with $p = 3.80$. In bulk, the hydrodynamic radius of the ellipsoidal fusion product is 4% larger than the hydrodynamic radius of the spherical fusion product.[5,12]

The dimer state consists of two identical spheres with diameters $\bar{d}_{\text{before}}$, i.e., with surface area $2A_{\text{before}}$ and $2V_{\text{before}}$. For a dimer in bulk, practically exact results are available for the hydrodynamic radius (see, e.g., Reference[13] or Reference[11] Table 1). Averaging over the three spatial dimensions gives $r_{\text{hyd}}^{\text{dimer}} = 1.392 r_0$, where r_0 is the radius of the individual spheres forming the dimer. A sphere with the same surface area as the dimer, i.e., $A = 2(4\pi r_0^2)$, has a radius of $r_{\text{sph.}} = \sqrt{A/(4\pi)} = \sqrt{2} r_0 \sim 1.41\, r_0$. So the hydrodynamic radius of a dimer is

98% of the radius of a sphere with the same area.

For ellipsoids confined between parallel walls, only approximate analytic results with a limited range of validity [5] and experimental data for selected parameters are available. [14] So we cannot approximate the fusion products with ellipsoids and fit our data. A complete analysis would also include how the shape of the liposomes affects the diffusiophoretic velocity.

In conclusion, for diffusion in bulk holds that the hydrodynamic radius of a non-spherical fusion product (the prolate ellipsoid) is larger than the hydrodynamic radius of a sphere with the same area.

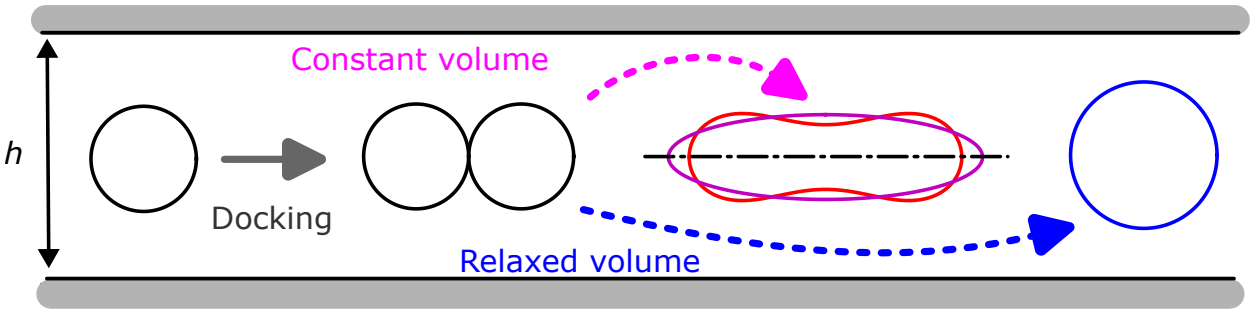

Sphere	**Dimer**	**Constant Vol.**	**Ellipsoid**	**Relaxed Sphere**
Volume V	2 V	2 V	2 V	$2\sqrt{2}$ V
Area A	2 A	2 A	2 A	2 A

Figure ESI-2: The initial, spherical liposome has a diameter $\bar{d}_{\text{before}} = 124\,\text{nm}$, a surface area A_{before}, and a volume V_{before}. The three fusion products all have a surface area $2A_{\text{before}}$, and the volumes are stated on the figure. The 'conserved volume' vesicle is a solution to the spontaneous curvature model for zero curvature and volume $2V_{\text{before}}$ (red),[10] and the purple figure is a prolate ellipsoid. The horizontal, dashed-dotted line is the axis of rotation of the vesicles. All vesicles are placed in a nanochannel with a height $h = 295\,\text{nm}$ and drawn to scale.

Loss of charge during fusion

Figure 4c in the main text shows that the zeta potential of the fusion product is lower than the zeta potential of the initial liposomes, indicating a loss of charge in the fusion process. This effect is investigated by performing experiments using liposomes without membrane fluorophores. Both A- and D-liposomes are prepared with 50 DNA probes, but half of the

probes on the A-liposomes are hybridized with an Atto-590 labeled target. In absence of D-liposomes, the A-liposomes give a constant fluorescence signal (Fig. ESI-1, 'Control'). After D-liposomes are introduced and fusion starts (time $t = 0$), the fluorescence intensity decreases and reached after $\sim$ 10 minutes a plateau value 15% to 20% below the initial intensity. The decrease is much smaller than expected from a replacement of the complementary target by the hybridization of all probes to the complementary DNA probes from the D-liposomes (50%). This indicates that even if some probes fall off during fusion and diffuse out of the trap, this must have a minimal effect on the zeta potential. Moreover, a loss of 15-20% of the negatively charge probes can only explain $\sim$5% of the observed change in zeta potential, prompting further experiments on the role of the DNA probes after fusion.

Another effect that can influence the zeta potential is that the DNA molecules have single-stranded overhangs before fusion, but are exclusively double-stranded after fusion. This could alter the zeta potential without changing the total number of DNA base pairs on the liposome surface. It was indeed previously observed that the change in zeta potential induced by DNA hybridization is different from adding single-stranded DNA probes.[2] We speculate that for a constant number of charges, as in the present fusion experiments, screening effects dominate the change in zeta potential.

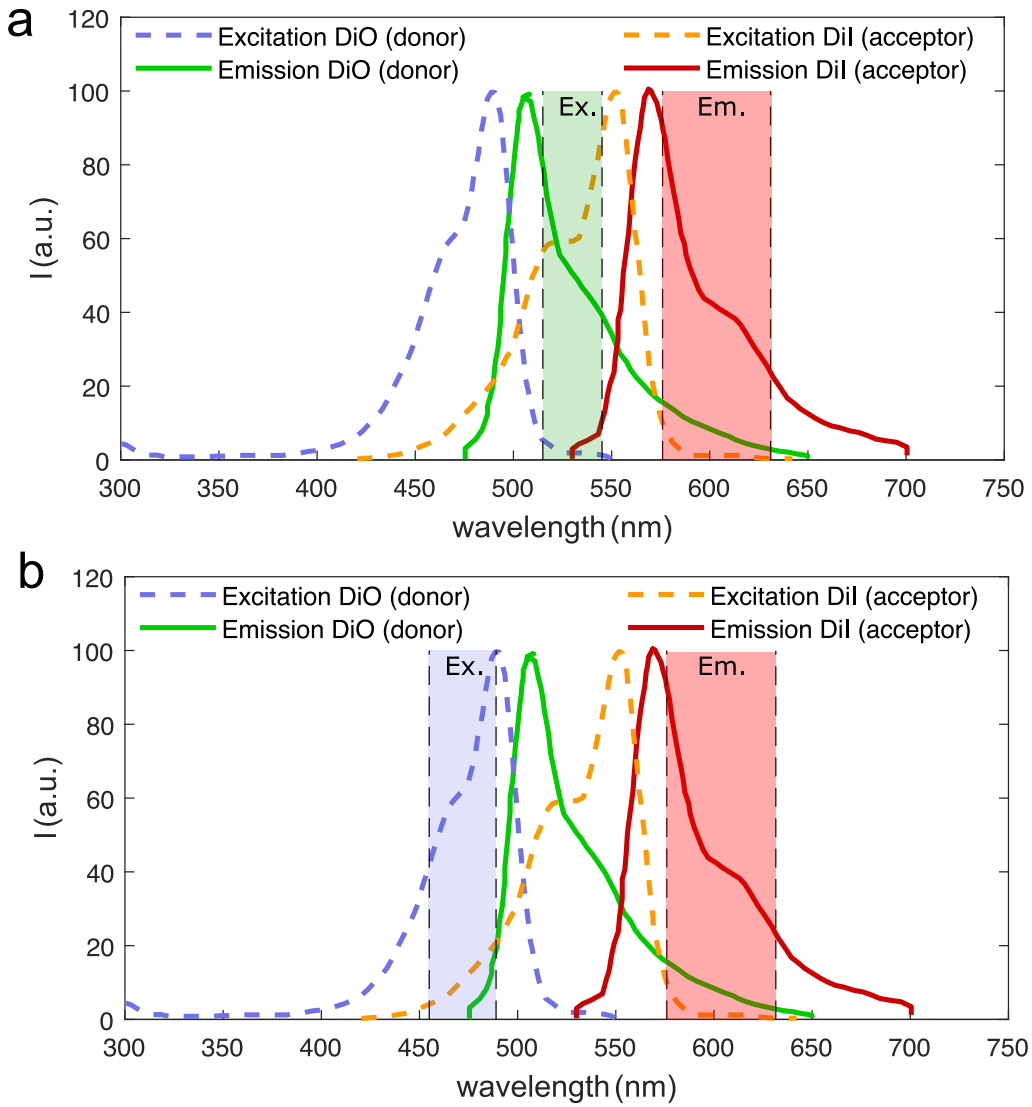

Figure ESI-3: Spectra of the excitation (Ex.) and emission (Em.) filters used for imaging the acceptor dye. (a) Green excitation of only the FRET-acceptor dye [Fig. 2(f) and Fig. 4(a) in the main text]. (b) Blue excitation of only the FRET-donor dye [Fig. 2(f) and Fig. 4(a) in the main text].

Simulated FRET intensities and standard errors on r_{fusion}

The data in Fig. 3(a)-(e) in the main text are from single experiments. As the arrival of D-liposomes in the trap and the fusion with A-lipsomes are stochastic processes, these FRET intensity traces will vary between repetitions of the same experiment. Moreover, the data points in the intensity traces are correlated, which complicates fitting with standard fitting

routines that often assume independent data. Here we determine the standard error on the fitted parameter r_{fusion} by simulating intensity traces. Each intensity trace is fitted to the same theoretical model as the experimental data to estimate r_{fusion}. The standard deviation of the fitted values for r_{fusion} is reported as the standard error on r_{fusion} in Fig. 3(f) in the main text.

We simulate the coupled eqn (1) and (2) in the main text using the exact Gillespie algorithm.[15] The parameters for the simulations are shown in the left-hand side of Table ESI-1 and in the caption. Each trace is fitted in the same way as the experimental traces, and the fitted value of r_{fusion} is recorded. The mean, the standard deviation, and their ratio are shown for each parameter set in the right-hand side of Table ESI-1. The deviation between $r_{\text{fusion}}^{\text{exp.}}$ and $\bar{r}_{\text{fusion}}$, see, e.g., $n = 100$, is due to a skewed distribution of the fitted fusion rates.

Simulations also show that the standard errors on the fitted values can be significantly reduced with a higher number of initially trapped A-liposomes. For example, if N_A^0 is doubled, but all other parameters are set as in Table ESI-1, the relative standard error for $n = 100$ is reduced to $\sigma_{r_{\text{fusion}}}/\bar{r}_{\text{fusion}} = 3.5\%$.

Table ESI-1: Parameters and results for the simulated FRET intensity traces. Here $r_{\text{fusion}}^{\text{exp.}}$ is the fitted fusion rates for the traces in Fig. 3(a)-(e) in the main text, which are used as input for the simulations. The common parameters for all simulations are set as in experiment, i.e., $r_{\text{in},D} = 0.9\,\text{s}^{-1}$, $\Delta t_{\text{add},D} = 14\,\text{min.}$, the sampling time is 20 s, and the total measurement time is 40 min. The number of simulations is 1000 for each parameter set. For the results, $\bar{r}_{\text{fusion}}$ and $\sigma_{r_{\text{fusion}}}$ are the mean and standard deviation of the fitted fusion rates.

n	N_A^0	$r_{\text{fusion}}^{\text{exp.}}$ $[10^{-4}\,\text{s}^{-1}]$	$\bar{r}_{\text{fusion}}$ $[10^{-4}\,\text{s}^{-1}]$	$\sigma_{r_{\text{fusion}}}$ $[10^{-5}\,\text{s}^{-1}]$	$\sigma_{r_{\text{fusion}}}/\bar{r}_{\text{fusion}}$ [%]
10	440	0.0244	0.0245	0.027	11
25	454	0.121	0.122	0.13	11
50	590	0.303	0.314	0.65	21
75	448	1.05	1.12	4.0	36
100	461	1.31	1.50	7.1	47

Negative control experiment for FRET data.

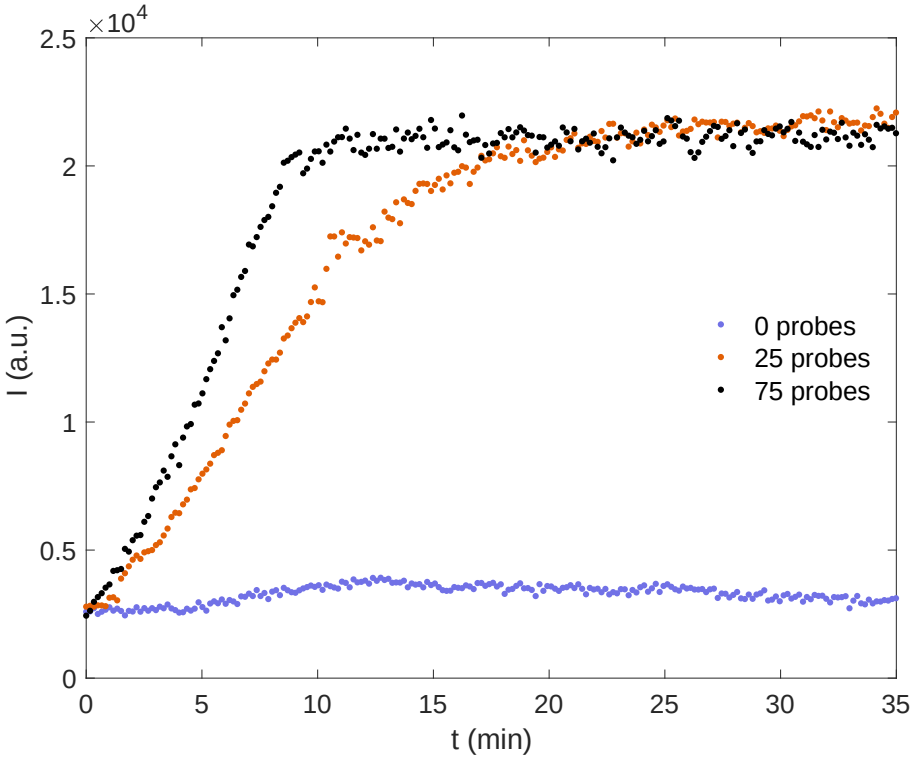

Figure ESI-4: Negative control of the FRET assay showing the recorded FRET intensity versus time for liposomes with 0, 25, and 75 DNA probes. In absence of probes, only a constant background signal is recorded. This is consistent with the assumption that fusion does not occur without DNA probes. The data for 25 and 75 DNA probes are the same as in Fig. 3(b) and 3(d) in the main text, but with no background subtracted.

Supplementary References

(1) Rasmussen, M. K.; Pedersen, J. N.; Marie, R. Size and surface charge characterization of nanoparticles with a salt gradient. *Nature communications* **2020**, *11*, 1–8.

(2) Rasmussen, M. K.; Pedersen, J. N.; Marie, R. Label-Free Sensing of Biorecognition on Liposomes. *ACS Sensors* **2020**, *5*, 4057–4063.

(3) Prieve, D. C.; Anderson, J. L.; Ebel, J. P.; Lowell, M. E. Motion of a particle generated

by chemical gradients. Part 2. Electrolytes. *Journal of Fluid Mechanics* **1984**, *148*, 247–269.

(4) Lee, C.; Cottin-Bizonne, C.; Biance, A.-L.; Joseph, P.; Bocquet, L.; Ybert, C. Osmotic flow through fully permeable nanochannels. *Physical Review Letters* **2014**, *112*, 244501.

(5) Happel, J.; Brenner, H. *Low Reynolds Number Hydrodynamics*; Prentice Hall, 1965.

(6) Miyamura, A.; Iwasaki, S.; Ishii, T. Experimental wall correction factors of single solid spheres in triangular and square cylinders, and parallel plates. *International Journal of Multiphase Flow* **1981**, *7*, 41–46.

(7) van der Sman, R. Drag force on spheres confined on the center line of rectangular microchannels. *Journal of Colloid and Interface Science* **2010**, *351*, 43–49.

(8) Stengel, G.; Simonsson, L.; Campbell, R. A.; Hook, F. Determinants for membrane fusion induced by cholesterol-modified DNA zippers. *Journal of Physical Chemistry B* **2008**, *112*, 8264–8274.

(9) Chan, Y.-H. M.; van Lengerich, B.; Boxer, S. G. Effects of linker sequences on vesicle fusion mediated by lipid-anchored DNA oligonucleotides. *Proceedings of the National Academy of Sciences* **2009**, *106*, 979–984.

(10) Seifert, U.; Berndl, K.; Lipowsky, R. Shape transformations of vesicles: Phase diagram for spontaneous- curvature and bilayer-coupling models. *Phys. Rev. A* **1991**, *44*, 1182–1202.

(11) Carrasco, B.; García de la Torre, J. Hydrodynamic Properties of Rigid Particles: Comparison of Different Modeling and Computational Procedures. *Biophysical Journal* **1999**, *76*, 3044–3057.

(12) Pencer, J.; White, G. F.; Hallett, F. R. Osmotically Induced Shape Changes of Large

Unilamellar Vesicles Measured by Dynamic Light Scattering. *Biophysical Journal* **2001**, *81*, 2716–2728.

(13) Swanson, E.; Teller, D. C.; de Haën, C. The low Reynolds number translational friction of ellipsoids, cylinders, dumbbells, and hollow spherical caps. Numerical testing of the validity of the modified Oseen tensor in computing the friction of objects modeled as beads on a shell. *The Journal of Chemical Physics* **1978**, *68*, 5097–5102.

(14) Han, Y.; Alsayed, A. M.; Nobili, M.; Zhang, J.; Lubensky, T. C.; Yodh, A. G. Brownian Motion of an Ellipsoid. *Science* **2006**, *314*, 626–630.

(15) Gillespie, D. T. Exact stochastic simulation of coupled chemical reactions. *The Journal of Physical Chemistry* **1977**, *81*, 2340–2361.